Available online at www.sciencedirect.com
ScienceDirect
Trans. Nonferrous Met. Soc. China 34(2024) 1393−1412
Transactions of Nonferrous Metals Society of China
www.tnmsc.cn

Design of fully-metallic phase change composites from thermodynamic calculations to experimental characterization of form-stable systems

Chiara CONFALONIERI, Alessandra CAMNAGHI, Elisabetta GARIBOLDI

Politecnico di Milano, Department of Mechanical Engineering, Via La Masa 1, 20156 Milan, Italy

Received 17 November 2022; accepted 30 June 2023

Abstract: Composite phase change materials (C-PCMs) for thermal energy management exploit the reversible phase transition (e.g., melting−solidification) of their one or more low-melting active phases to store and release thermal energy as latent heat. At the same time, the high-melting passive phases can provide additional properties, like form-stability and enhanced thermal conductivity. Fully-metallic composite systems with these features can be obtained from immiscible alloys. In this work, thermodynamic calculations and experimental tests are combined to explore the potential of a set of binary (Al−In, Al−Sn, Al−Bi and Cu−Bi) and ternary (Al−In−Sn and Al−Bi−Sn) immiscible alloys for their use as C-PCMs in a temperature range between 100 and 300 °C. The results show that the combination of the two approaches proved to be necessary to have a full comprehension of the composite system and find the best solution for design requirements, overcoming the time-wasting "trial-and-error" approach and providing high-quality data for simulations.

Key words: composite phase change materials; alloy design; thermodynamic properties; form-stability; heat storage

1 Introduction

Fully-metallic composite materials can be designed from immiscible alloys, i.e., metallic systems consisting of two or more phases which do not interact at least in a specific composition and/or temperature interval. According to thermodynamics, a miscibility gap occurs when a multi-component system cannot minimize its Gibbs free energy of mixing by forming a solid solution [1]. Immiscible alloys are frequently used in bearings, thanks to their dual-phase and hard-soft microstructure without large interdendritic spacing [2,3]. The hard matrix sustains the loads, while soft particles provide solid lubrication properties, embedding the particles generated by wear phenomena [4,5]. Typical systems are Al alloys with Sn [6−9], Pb [10] and Bi [4,5,11], in binary, ternary or more elements alloys. For example, YUAN et al [12] studied the effect of Si in Al−Sn alloys to improve load bearing and fatigue resistance, while ZHAI et al [13] focused on the addition of Sn in Al−Cu alloys to promote the formation of a homogeneous phase distribution; an overview of element addition and heat treatment effects on mechanical and tribological properties of Al−Sn alloys was proposed by BHAT et al [14].

This multi-phase microstructure is also suitable for phase change materials (PCMs) for thermal energy management applications. These functional materials store thermal energy as latent heat during an endothermic phase transition (e.g., melting); then, as the transition is reversed, they release the stored energy. Composite PCMs (C-PCMs) consist of an active phase that undergoes the phase transition, and a high-melting passive phase that provides additional features of structural and thermal properties,

Corresponding author: Chiara CONFALONIERI, E-mail: chiara.confalonieri@polimi.it
DOI: 10.1016/S1003-6326(24)66479-4

such as thermal conductivity or heat capacity. Thermal conductivity of the system controls the heat transfer rate, affecting the PCM efficiency, as discussed by YUAN et al [15]. Further, the combined heat capacity of the two phases affects the sensible heat storage before and after transition. If solid−liquid transitions are involved, the passive phase could also prevent the leakage of molten active phase and keep material shape throughout the phase change. This form-stability depends on the wettability of molten active phase on the passive one. Good wettability ensures bonding between the phases thanks to long range interactions, achieving form-stability at least in low loading conditions; an example is the Cu−Bi system studied by SINGH et al [16]. Conversely, if wettability is poor, active phase can be physically embedded within a continuous passive matrix, which can also enhance system thermal conductivity. As reported and investigated by CONFALONIERI et al [17] and SUGO et al [18], examples of metallic C-PCMs are Al−Sn, Fe−Cu, Fe−Mg and Al−Bi, where the second element is the active phase.

PCMs design is usually based on literature properties, theoretical calculations/simulations and "trial-and-error" experiments. Key properties are transition temperature and latent heat, thermal conductivity and stability over thermal cycles. In the last decade, several literature reviews collected selection strategies and main properties for PCM design: ZHOU and WU [19] and WEI et al [20] focused on medium- and high-temperature PCMs, COSTA and KENISARIN [21] and WANG et al [22] reviewed metallic PCMs, including immiscible alloys. These works are good starting points to select PCMs; however, they usually report properties at a specific temperature and not as function of temperature, which is necessary to evaluate PCM performance precisely. Moreover, it is often complex to retrieve all the properties of interest in literature. Also, literature data are usually limited to the active phase material and not on the possible containers. In this perspective, RAWSON et al [23] conducted thermodynamic calculations with CALPHAD method, to obtain properties for metallic PCMs with eutectic compositions, validating results with literature data. The PCM-container compatibility was assessed by analyzing miscibility gaps in pseudo-binary diagrams, considering that a compatible container phase will not interact with the PCM [23]. However, this work does not evaluate the overall system properties (container + PCM). GHERIBI et al [24] applied the CALPHAD method to calculate properties of salt-based systems not available in literature. They proposed an optimization problem to satisfy design requirements and gave a preliminary evaluation of container corrosion; however, as RAWSON et al [23], GHERIBI et al [24] did not consider the container contribution to the overall system properties.

An original design approach is proposed for metallic C-PCMs in the present study. Firstly, this method applies thermodynamic calculations with CALPHAD method and physical models to evaluate properties throughout the C-PCM temperature application range for both the active phase (temperature and latent heat) and the overall system (specific heat capacity, density and thermal diffusivity). A preliminary literature survey allowed to select immiscible alloys manufactured with powder metallurgy processes, thus obtaining a homogeneous phase distribution and a potential form stability when used as PCMs. The research focused on Al alloys for their good thermal conductivity and low density with respect to other alloys, like Cu alloys. Al-based binary and ternary alloys were selected with Sn, Bi, In, In−Sn and Bi−Sn as active phases in various volume fractions. They have active phase transition temperatures between 100 and 300 °C, and this range is intermediate between transition temperatures of most low-melting polymeric and organic PCMs (from −40 to 120 °C) and the high-melting inorganic PCMs, like molten salts and metals (e.g., Al−Cu based alloys and pure Al, from 550 to 660 °C). In addition, Cu−Bi system was considered as system with form-stability due to high wettability, instead of physical confinement. By repeating calculations iteratively for different compositions, it is possible to find the best alloy composition for the design requirements, following the "alloy-by-design" method, as applied by GHERIBI et al [24] and REED et al [25].

In this work, some alloys were then produced by powder metallurgy (powder mixing, compression and sintering) according to previous studies [26,27]. This production process prevents segregation of active phase at grain boundaries of high-melting phase and inside the specimen, as it happens with simple cooling of cast immiscible alloys. Other

solutions could be rapid solidification processes, like laser melting of powders [28,29] or melt spinning [2], and casting with inoculants or grain refiners [8,30]. Microstructural, thermal and mechanical characterization was performed. Specifically, thermal characterization focused on transition temperature and latent heat, as well as thermal diffusivity and thermal expansion.

2 Experimental

2.1 Alloy design

The design process of metallic C-PCM based on multiphase immiscible alloys will consider the following requirements: (1) Passive phase and active phase should be completely immiscible in the whole application temperature range; therefore, a "safe" composition range should be selected. (2) Each component (passive phase or active phase) can be an alloy itself, as long as there are not interactions between elements belonging to the passive phase and the active phase, respectively. An alloy-based active phase can potentially undergo more than one transition in the temperature/composition range of immiscibility. (3) The storable energy should be maximized, balancing this requirement with the ones for other properties (e.g., high thermal conductivity and low density). (4) The quantity of active phase should be suitable to avoid percolation and keep form stability even when the active phase is molten (e.g., forming isolated particles or allowing enough surface interaction).

The first three requirements can be evaluated through thermodynamic calculations, which in the present study were performed with Thermo-Calc software [31,32]. Phase diagrams show the immiscibility range, both in terms of composition and temperature. Then, thermodynamic properties, as transition temperature, latent heat of transition, enthalpy of the system, specific heat capacity and specific volume as function of temperature, can be calculated in the range of interest with a one-axis calculation. Additional properties can be calculated from thermodynamic properties, e.g., density (inverse of specific volume), or applying models to literature data, as for thermal conductivity (e.g., rule of mixtures [33], Maxwell-type models [34], Bruggeman model [35] and Progelhof model [36]). Once calculations are completed for some reference compositions, the trend of each property with composition is known, allowing a more focused selection of optimal active/passive phase ratio. The fourth requirement, regarding compositional and shape stability, could be faced with a percolation study. This can be complex, especially for the present case since the embedded phase usually has an irregular shape. In the first stage, considering also literature works about percolation by RAWSON et al [37], a conservative limit for active phase volume fraction can be 40%.

In the present study, four binary systems (Al−Sn, Al−In, Al−Bi and Cu−Bi) and two ternary systems (Al−In−Sn and Al−Bi−Sn) with Al or Cu as high-melting phase were selected as candidates based on the preliminary literature review presented in the introduction. Useful reference properties for each element are reported in Table 1. In the two proposed ternary systems, the active phase consists

Table 1 Properties of pure elements behaving as passive or active phase in proposed PCM alloys

Property	Passive phase		Active phase		
	Al	Cu	Sn	In	Bi
Density at RT/(g·cm^3)	2.699 [38]	8.96 [38]	7.298 [38]	7.29 [39]	9.8 [39]
Melting temperature/°C	660.3 [38]	1084.6 [38]	231.9 [38]	156.3 [39]	271.3 [39]
Latent heat of melting per unit mass/(kJ·kg^{-1})	397 [38]	209 [38]	60 [38]	28 [39]	50 [39]
Latent heat of melting per unit volume/(J·cm^{-3})	1071	187	438	207	492
Thermal conductivity at RT/(W·m^{-1}·K^{-1})	237 [38]	401 [38]	67 [38]	82 [40]	10 [41]
Thermal diffusivity at RT/(cm^2·s^{-1})	0.972	1.162	0.399	0.480	0.082
Coefficient of thermal expansion (0−100 °C)/10^{-6} K^{-1}	23 [38]	16 [38]	21 [38]	33 [42]	13 [41]
Specific heat capacity at RT/(J·g^{-1}·K^{-1})	0.903 [38]	0.385 [38]	0.229 [38]	0.234 [39]	0.124 [39]

Latent heat of melting per unit volume was calculated through multiplying latent heat of melting per unit mass by density. Thermal diffusivity at room temperature (RT) was calculated through dividing thermal conductivity by specific heat capacity and density

of two elements which are mutually miscible, and both immiscible with Al passive phase. The binary In−Sn and Bi−Sn systems, chosen as active phase, undergo a eutectic transformation. If eutectic composition is chosen, the phase transition will occur at constant temperature, i.e., solidus and liquidus temperatures coincide throughout the transition.

Thermo-Calc database for Al-based alloys was used [32]. Calculation parameters were ambient pressure and temperature range of 20−300 °C with steps of 5 °C. For each binary system, calculations were performed on five alloys, with 5%, 10%, 20%, 30% and 40% in volume fraction of active phase. Since mass fraction is more convenient for production purposes, the alloy compositions were converted from volume fraction to mass fraction according to Eq. (1):

$$w_{\mathrm{A}}=\frac{\rho_{\mathrm{A}}\varphi_{\mathrm{A}}}{\left(\rho_{\mathrm{A}}-\rho_{\mathrm{P}}\right)\varphi_{\mathrm{A}}+\rho_{\mathrm{P}}} \tag{1}$$

where w_{A} is the mass fraction and φ_{A} is the volume fraction of low-melting active phase, while ρ_{A} and ρ_{P} are densities for active phase and passive phase, respectively. For ternary systems, the active phases with eutectic composition (In−51%Sn and Bi−55%Sn in mass fraction) were combined with Al; as done with binary systems, the active phase volume fractions were 5%, 10% and 20%. In addition, the binary active phase mass fraction was fixed to 40% and calculations were repeated for different compositions of the active phase itself, i.e., in correspondence of eutectic composition as well as below and above it. Thermal conductivity range of the composite materials was estimated with the mixture rule for upper ($k_{\mathrm{c,u}}$, Eq. (2)) boundary and lower boundary ($k_{\mathrm{c,l}}$, Eq. (3)) [33]:

$$k_{\mathrm{c,u}}=k_{\mathrm{P}}\varphi_{\mathrm{P}}+k_{\mathrm{A}}\varphi_{\mathrm{A}}=k_{\mathrm{A}}+\left(k_{\mathrm{P}}-k_{\mathrm{A}}\right)\varphi_{\mathrm{P}} \tag{2}$$

$$k_{\mathrm{c,l}}=\frac{k_{\mathrm{P}}k_{\mathrm{A}}}{k_{\mathrm{P}}\varphi_{\mathrm{A}}+k_{\mathrm{A}}\varphi_{\mathrm{P}}}=\frac{k_{\mathrm{P}}k_{\mathrm{A}}}{k_{\mathrm{P}}+(k_{\mathrm{A}}-k_{\mathrm{P}})\varphi_{\mathrm{P}}} \tag{3}$$

where k_{P} and k_{A} are the thermal conductivities of passive and active phases, respectively, and φ_{P} is the volume fraction of passive phase. Thermal conductivity values for pure elements are reported in Table 1. Average thermal diffusivity was calculated through dividing thermal conductivity by the product of specific heat capacity and density. This method will give consistent values of thermal conductivity resulting from the phase distribution that can be achieved experimentally with powder metallurgy. In fact, the composite materials in this study consist of a homogeneous dispersion of a significant volume of particles in another phase, with differences in their thermal conductivity not higher than one order of magnitude. In this case and for inclusion volume fraction lower than 40%, the approximation of the actual thermal conductivity to the average of the two equations is not far from the actual one, also for different arrangements of inclusions [43]. This approach is also supported by a previous study regarding an Al−Sn alloy [28], where thermal conductivity values, calculated by lattice Monte−Carlo method from real microstructures, were close to the average between the two boundaries.

2.2 Alloy production

Samples were produced from powders of pure elements: Al (99.7% in mass fraction, size <45 μm, ECKA Granules Germany GmbH), Cu (99.95% in mass fraction, particle size distribution of 0.5−11 μm with an average size of 3.4 μm, m4p material solutions GmbH), Sn (99.85% in mass fraction, 100 mesh, Thermo Fisher (Kandel) GmbH, Alfa Aesar), In (99.99% in mass fraction, Merck Life Science Srl), and Bi (99.85% in mass fraction, 150 μm, Thermo Fisher (Kandel) GmbH, Alfa Aesar). Before the mixing processes, powders were sifted with a 63 μm sieve, to remove coarse particles and agglomerates. For all the alloys, the active phase was blended with the passive phase (Al or Cu) through simple mixing in a tumbler mixer at room temperature and 25 r/min for 1 h. In the cases of ternary systems, the active phases with eutectic composition (In−51%Sn and Bi−55%Sn, in mass fraction) were produced by ball-milling the powders of the active phase elements, to obtain mechanical alloying before simple mixing with Al. Ball milling was performed using a planetary mill (Retsch PM 400 Planetary Ball Mill) with hardened steel balls with a diameter of 20 mm (material-to-ball mass ratio 1:4) for 90 min, alternating 20 min of milling and 10 min of pause. Atmosphere in the ball milling jar was argon, and ethanol (7% in mass fraction) was added as a lubricant.

Then, blended powders were compressed in three steps at room temperature with the maximum pressure of 300 MPa held for about 1 min, as in an earlier study [27]. Finally, samples were sintered in

pure Ar atmosphere to prevent oxidation. Samples containing Al with Sn, Bi or Bi−Sn were sintered at 500 °C for 1 h, with an intermediate holding at 200 °C for 30 min to promote the relaxation of the high-melting phase. All the other samples were sintered at 350 °C for 1 h, with intermediate holding at 140 °C for In-containing alloys and at 240 °C for Cu−Bi alloys. Production process steps and their parameters are summarized in Table 2.

2.3 Alloy characterization

Analyses with scanning electron microscope (SEM, Zeiss Sigma 500) on mounted and polished samples aimed at studying microstructural features, detecting backscattered electrons (BSE), and determining composition with energy dispersive X-ray spectrometry (EDS).

Density was measured using Archimedes' method (Analytical balance ME204 with density kit standard and advanced, Mettler Toledo). The instrument resolution was 0.001 g/cm^3 and the measurement was repeated three times.

Transition temperature and latent heat were evaluated with differential scanning calorimetry (DSC, Setaram TG/DSC Labsys 1600) on samples of 50 mg (Al-based) or 100 mg (Cu-based); the mass difference for Al and Cu alloys is due to the difference in density and the need of having samples with similar volume to fit alumina crucibles. DSC tests consisted of two cycles between room temperature and 320 °C at 10 °C/min in argon atmosphere. The measurement of activation energy was calibrated using In, Sn and Zn reference standards.

Thermal expansion was evaluated with a vertical dilatometer (Linseis L75 VERT) in vacuum performing four thermal cycles at 10 °C/min from room temperature. The highest temperature for this test was selected according to the active phase material to reduce the risk of leakage, holding it above melting temperature for an excessively long time: In 200 °C, Sn and In−Sn 270 °C, and Bi 320 °C. The instrument error on sample length variation depends on the actual sample length and can be considered less than 0.03 μm. Coefficient of thermal expansion (CTE) between the ambient temperature (T_0, 20 °C) and the temperature (T_1) was calculated with the definition given in ASTM E228 specification [44]:

$$(\mathrm{CTE})_{T_1} = \frac{1}{L_0}\cdot\frac{\Delta L}{\Delta T} = \frac{1}{L_0}\cdot\frac{L_1 - L_0}{T_1 - T_0} \tag{4}$$

where L_0 is the initial length of the sample and L_1 is the sample length at temperature T_1. To evaluate the effect of active phase transition on CTE, the average of CTE values between room temperature and transition temperature was compared with the average of CTE values above transition temperature during heating part of test cycle. The presented values are the average of all cycle repetitions for each alloy.

Thermal diffusivity was measured during a single thermal cycle between room temperature and 320 °C using laser flash analysis method in vacuum (Linseis LFA 1000/1600). The error on the measurement is about 5% for alloys without phase transitions; close to phase transitions, the margin of error is expected to be slightly higher.

Table 2 Summary of powder metallurgy process steps and parameters for each PCM system (The melting temperature of each phase is reported as reference with respect to process temperatures)

System composition (Transition temperature)*		Powder mixing	Compression	Heat treatment temperature/°C	
High-melting phase	Low-melting phase (PCM)			Intermediate holding (30 min)	Sintering (1 h)
Cu (1085 °C)	Bi (271 °C)	Simple mixing	Room temperature, maximum pressure: 300 MPa	240	350
Al (660 °C)	Sn (232 °C)	Simple mixing	Room temperature, maximum pressure: 300 MPa	200	500
	Bi (271 °C)			200	500
	In (156 °C)			140	350
	Bi−Sn (141 °C)	Ball milling on PCM + simple mixing	Room temperature, maximum pressure: 300 MPa	200	500
	In−Sn (117 °C)			140	350

* Pure element melting temperatures are the same literature values in Table 1; values for Bi−Sn and In−Sn refer to eutectic composition and were determined in thermodynamic calculations

A preliminary evaluation of mechanical properties was done by means of Vickers micro-hardness (Future-tech FM−700 microhardness tester), repeating 5 measurements with a load of 4.91 N and a dwell time of 15 s on a metallographically prepared surface parallel to compression direction.

3 Results

3.1 Properties calculation

3.1.1 Binary systems and ternary systems with eutectic active phase

Calculated transition temperatures are reported in Table 3 for the binary systems and the ternary systems with ratio between active phase elements corresponding to eutectic composition, i.e., In−51%Sn and Bi−46%Sn in mass fraction.

Transition temperatures for binary alloys are almost equal to melting temperatures of pure active phases (Table 1), with a little reduction for Sn and Bi alloys. As expected, active phases with eutectic composition have a lower transition temperature with respect to the pure elements of which they are composed.

To evaluate the thermal energy storage performance of the six systems, it is useful to analyze the storable energy in a common temperature interval. This definition of storable energy includes both the latent heat associated to transition and the sensible heat due to temperature variation, depending on specific heat capacity as well. This approach allows to compare systems that undergo transition at different temperatures, and it is also more practical to select a material for industrial applications in devices for thermal energy storage or management. The considered temperature range is between 100 and 300 °C, which includes all the transition temperatures of the studied systems. Storable energy values per unit volume and per unit mass as function of transition temperature are shown in Fig. 1(a).

For all the investigated alloys, the storable energy per unit volume is higher than the corresponding storable energy per unit mass. Values of storable energy per unit mass are close for Al-based alloys with different active phases, but the same volume fraction. On the other hand, as active

Table 3 Calculated transition temperatures with Thermo−Calc software

System	Al−In	Al−Sn	Al−Bi	Cu−Bi	Al−$(In−Sn)_{eu}$	Al−$(Bi−Sn)_{eu}$
Transition temperature/°C	156.40	229.45	270.18	270.40	116.76	141.40

For ternary systems of Al−In−Sn and Al−Bi−Sn, the ratio between active phase elements corresponds to eutectic composition (In−51%Sn and Bi−46%Sn in mass fraction, respectively)

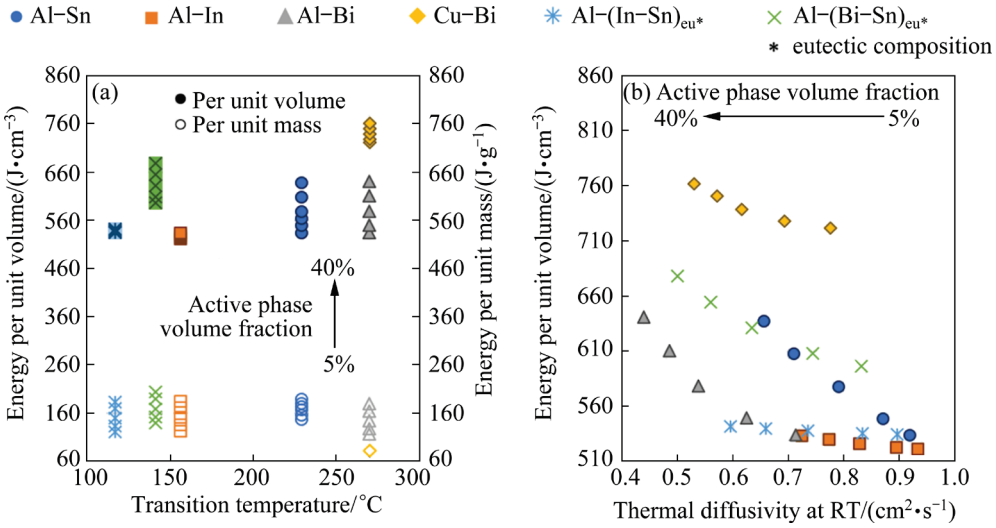

Fig. 1 Storable energy in temperature range of 100−300 °C, including both sensible and latent heat contributions for all investigated systems (For ternary ones the active phase has eutectic composition. Each point represents an alloy with different active phase volume fractions increasing as indicated by the arrows (5%, 10%, 20%, 30%, and 40%)): (a) Storable energy per unit volume (colored marker) and per unit mass (white marker) as function of transition temperature; (b) Storable energy per unit volume as function of thermal diffusivity at RT

phase content changes, the variation of energy storage per unit volume is wider for Al−Sn, Al−Bi and Al−$(Bi−Sn)_{eu}$ than for Al−In and Al−$(In−Sn)_{eu}$. Comparing the alloys with Bi as active phase, the system with Al as passive phase can store higher energy per unit mass, but lower energy per unit volume with respect to the one with Cu as passive phase.

Focusing on ternary systems, besides lower transition temperature with respect to the binary systems with the same elements, the addition of a third element changes the storable energies as well. In terms of energy per unit mass, variations are quite limited, while they are more evident for energy per unit volume with different behaviors between Al−(In−Sn) and Al−(Bi−Sn). Storable energy per unit volume in Al−(In−Sn) is slightly higher than that of Al−In (about 2%), and it varies in a narrow range with the active phase volume faction, as for Al−In. On the other hand, with respect to Al−Sn, storable energy per unit volume is lower from 2% up to 17% as active phase volume fraction increases from 5% to 40%. Considering Al−(Bi−Sn) system, storable energy per unit volume is higher in the ternary system with respect to Al−Sn and Al−Bi systems (which can store almost the same energy with the same active phase content), with variations from 5% to 10% depending on active phase quantity.

In Fig. 1(b), storable energy per unit volume between 100 and 300 °C is shown as function of thermal diffusivity at room temperature. For the same system, thermal diffusivity increases as the active phase volume fraction decreases. Comparing different systems, the ones containing Bi show the lowest values of thermal diffusivity, but at the same time alloys with Bi, Sn or Bi−Sn can store more energy per unit volume with respect to In and In−Sn alloys with the same active phase volume fraction. Alloys with low quantity of active phase are an exception, since values of storable energy are close for Al-based alloys with In, Bi, Sn and In−Sn; further, excluding Al−Bi, they have also close values of thermal diffusivity.

The enthalpy of the system per unit volume as function of temperature shows how energy is stored as temperature increases; curves in Fig. 2 refer to 20% (volume fraction) of active phase in binary systems and ternary systems with eutectic active phase. The jump discontinuities correspond to phase transitions. For all the systems, the slope of the curves, i.e., the specific heat capacity (derivative of enthalpy with respect to temperature) multiplied by density, does not change significantly. Al-based systems have almost parallel curves. Comparing curves of Al−Sn, Al−Bi and Al−(Bi−Sn), it is possible to notice that before and after transitions they tend to overlap. On the other hand, curve of Al−(In−Sn) is always above Al−In curve, while it crosses Al−Sn curve during Sn phase transition at 229 °C being higher at low temperatures and lower at high temperatures. Cu−Bi alloy shows a completely different slope with respect to Al alloys, and it is above all the other curves at any temperature.

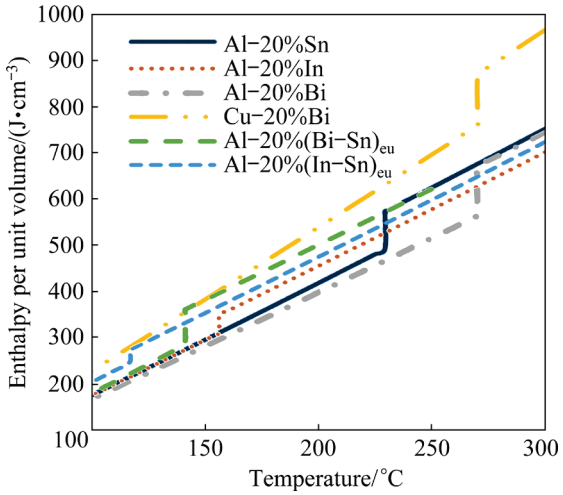

Fig. 2 Enthalpy of system per unit volume as function of temperature for all systems with 20% (volume fraction) of active phase (Ternary systems have active phase with eutectic composition; the jump discontinuities in the curves correspond to phase transitions)

3.1.2 Ternary systems with different active phase compositions

To study the effect of active phase composition on energy storage when it is not eutectic, mass fraction of active phase (In−Sn or Bi−Sn) in ternary systems was fixed at 40% and alloys with ipoeutectic, eutectic and ipereutectic compositions of the binary phase were selected for calculations. Thanks to the immiscibility of both elements of the active phase in Al (see phase diagrams for Al−In [45], Al−Bi [4] and Al−Sn [46]), the pseudo-binary phase diagram of the ternary system with fixed Al mass fraction (Figs. 3(a) and Fig. 4(a)), in the composition range of active phase (0−40%, mass fraction) and below active phase elements melting

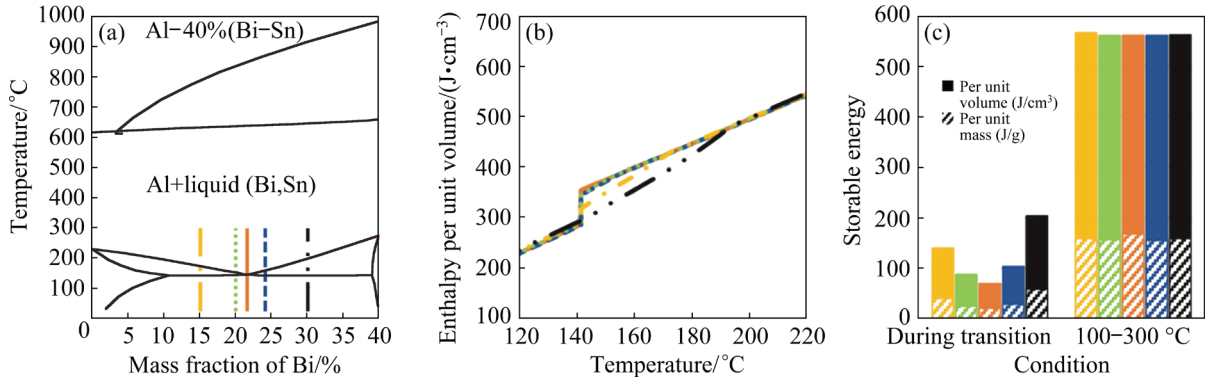

Fig. 3 Pseudo-binary phase diagram of ternary Al−Bi−Sn alloy with 40% (mass fraction of binary Bi−Sn active phase) calculated by Thermo−Calc [32] with vertical lines showing compositions of investigated alloys, with ipoeutectic (yellow dashed-dotted line and green dotted line), eutectic (orange solid line) and ipereutectic (blue dashed line and black dashed-double dotted line) active phase compositions (a), enthalpy per unit volume as function of temperature (b) (The legend of (b) is the same as that of (a)), and storable energy per unit volume or mass (c) for each alloy with the same color code (from left to right: two ipoeutectic, one eutectic and two ipereutectic active phase compositions)

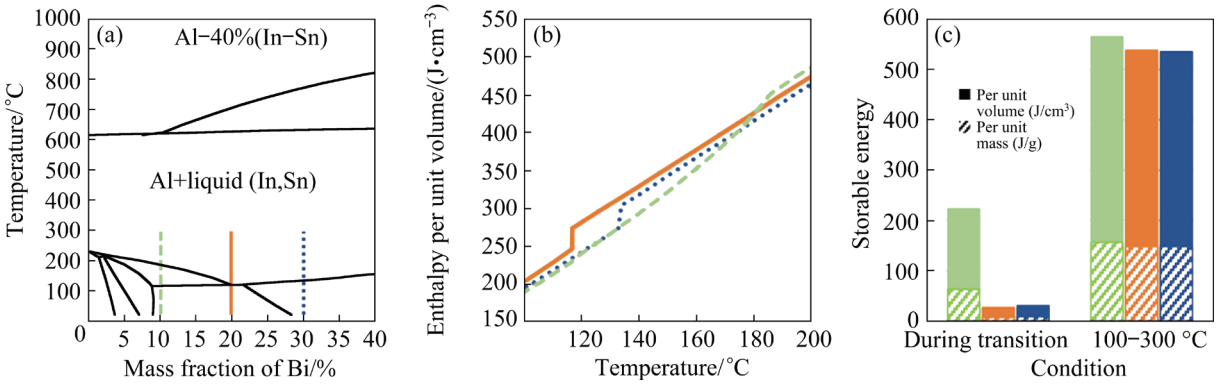

Fig. 4 Pseudo-binary phase diagrams of ternary Al−In−Sn alloy with 40% (mass fraction of binary In−Sn active phase) calculated by Thermo−Calc [32] with vertical lines showing compositions of investigated alloys with ipoeutectic (green dashed line), eutectic (orange solid line) and ipereutectic (blue dotted line) active phase compositions (a), enthalpy per unit volume as function of temperature (b) (The legend of (b) is the same as that of (a)), and storable energy per unit volume or mass (c) for each alloy with the same color code (from left to right: ipoeutectic, eutectic and ipereutectic active phase compositions)

temperature, resembles the binary phase diagram of the active phase elements (shown in [47]). Therefore, if the ternary system is considered, it is more precise to use the term “eutectoid”, instead of “eutectic”, since the Al phase is already solid. Nevertheless, since these ternary alloys are seen as two-phase composite materials based on Al and a binary alloy, throughout the paper the term “eutectic” is used with reference to the active phase binary system composition, even when ternary systems are discussed.

For the Al−Bi−Sn systems, an ipoeutectic alloy and an ipereutectic alloy were selected close to the eutectic composition, with 20% and 24% Bi in mass fraction, respectively. Comparing their enthalpy per unit volume in the transition temperature range (Fig. 3(b)), both curves almost overlap that of the alloy with eutectic active phase, and most of the transition occurs at constant temperature. For these non-eutectic compositions, the completion of transformation in heating occurs within 10 °C range above it. Moving away from the eutectic composition, both increasing and decreasing Bi content, the steep increase of enthalpy at transition onset reduces and enthalpy increases smoothly until curves overlap again, even with a higher slope. In terms of storable energy per unit volume during transition (Fig. 3(c)), the alloy with eutectic active phase has the lowest value, while storable energy increases as the composition moves away from

eutectic one. On the other hand, the storable energy in a wider temperature range (100−300 °C), is the almost the same for each alloy (Fig. 3(c)). The storable energy per unit mass (Fig. 3(c)) shows the same trends, but with lower values.

For Al−In−Sn system (Fig. 4(a)), the alloy with ipoeutectic composition of active phase shows the same behaviour observed for Al−Bi−Sn alloys far from eutectic composition, with smooth increase of enthalpy per unit volume with temperature (Fig. 4(b)) and higher energy can be stored during transition with respect to eutectic composition. On the other hand, as In mass fraction increases above eutectic composition value, solidus and liquidus lines for the active phase overlap (Fig. 4(a)). The corresponding curve of enthalpy (Fig. 4(b)) shows a steep increase upon phase transition, which is not perfectly vertical, but it has a remarkably high slope. Transition temperature (133 °C) is higher than that of eutectic composition (117 °C), but transition range is about 1 °C. Storable energy is thus quite the same as the energy of the alloy with eutectic composition. Considering the temperature range of 100−300 °C, the three alloys can store almost the same energy per unit volume or mass, as observed for Al−Bi−Sn system (Fig. 4(c)).

3.2 Alloy characterization

Every proposed system was produced in various compositions. For ternary systems, the alloys selected for production have the binary active phase with the nominal eutectic composition. During sample preparation for testing, Al-based alloys containing Bi showed an unexpected reaction with water, causing a strong heat release, the formation of bubbles in water and decomposition of the material. Therefore, it was not possible to prepare specimens for any of the planned tests. The manufacturing and use of Al−Bi-based C-PCM should be thus carefully considered for practical applications.

3.2.1 Microstructure

Microstructure was analyzed through SEM micrographs, taken from the core part of specimens. The lightest areas correspond to the active phase (In, Sn, In−Sn or Bi), the grey areas consist of the passive phase (Al or Cu), and the darkest areas are pores. SEM images of Al-based alloys are shown in Fig. 5. For all the alloys, active phase particles appeared quite isolated one another and pores, which were observed in every sample, and did not form a network as well. Some of the Al particles kept their spherical shape from powder form, as clearly visible especially in Al−Sn alloys by Sn and porosity at Al particle boundaries.

EDS measurements on Al-based alloys showed that they have only the elements of the nominal composition, sometimes with very little amounts of oxygen. Further, negligible or null quantities of Al were measured in active phase regions, and vice versa. Assuming that area fraction measured on micrographs corresponds to volume fraction, as suggested by UNDERWOOD [48], it is possible to evaluate the volume fractions of the three phases (Al, active phase and porosity) in the analyzed areas. As shown in the diagrams of Fig. 5, porosity ranges from 1% to 12%, without clear dependence on active phase volume fraction. The ratio of volume fraction between Al and active phase, even removing the contribution of porosity, is not always matching the nominal composition of the alloy, having higher or lower active phase content.

Focusing on the ternary Al−In−Sn alloy, a high magnification micrograph of an In−Sn particle is shown in Fig. 6. Light Sn-rich areas, with an approximately circular shape, can be observed, while regions at their boundaries are richer in In with still a significant amount of Sn. In both areas the fraction of Al is negligible.

Micrographs of Cu−Bi alloys are shown in Fig. 7. Although it is possible to clearly distinguish Bi-rich and Cu-rich regions, differently from Al-based alloys, Bi particles are not completely isolated, forming both Bi particles and a fine network around Cu particles. Dark areas are pores. EDS measurements confirmed the absence of diffusion of Cu in Bi, and vice versa. Phase volume fractions measured from images show porosity ranging from 2% to 13%, independently of the active phase volume fraction as in Al alloys. Active phase volume fraction is higher with respect to nominal composition for low Bi content and slightly lower for high Bi content.

3.2.2 Density

The density values for the studied materials experimentally measured with Archimedes' method are reported in Fig. 8 as a function of nominal active phase volume fraction. The theoretical (bulk) density values calculated with Thermo−Calc are indicated with dashed lines in the same plot.

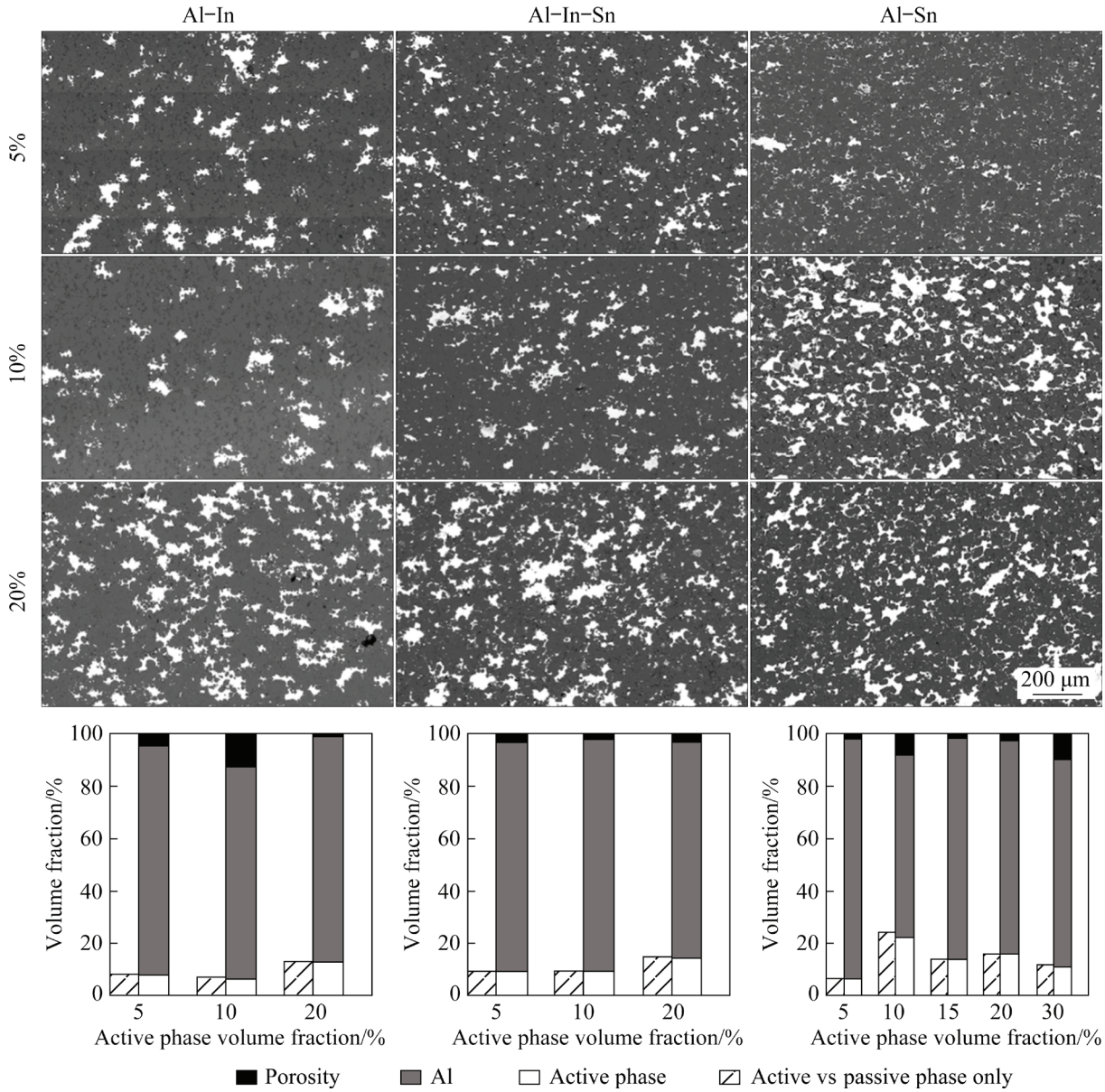

Fig. 5 SEM micrographs of Al-based alloys with different active phases (In, In−Sn and Sn) and nominal compositions (5%, 10% and 20% in volume fraction of active phase), and diagrams showing volume factions of phases (Al, active phase and porosity) measured from micrographs and percentage of active phase with respect to Al neglecting porosity

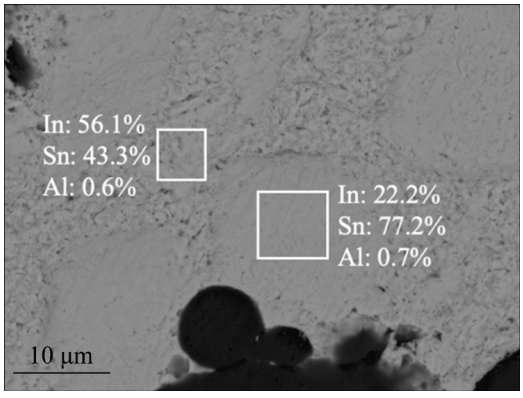

Fig. 6 High magnification SEM micrograph of In−Sn-rich particle, with EDS measurements in mass fraction

Standard deviation for experimental results is equal or lower than 1%, so it would not be visible on the plot.

Both theoretical and experimental curves for Al-based alloys (Al−Sn, Al−In and Al−In−Sn) overlap, with a positive trend as active phase volume fraction increases. Experimental values are 7%−16% lower than theoretical ones. Cu−Bi alloys have, as expected, higher densities with respect to Al-based ones (Fig. 8). Cu−Bi alloys also show an increase of density with active phase volume; however, the variation is less significant with respect to Al-based alloys since density values of

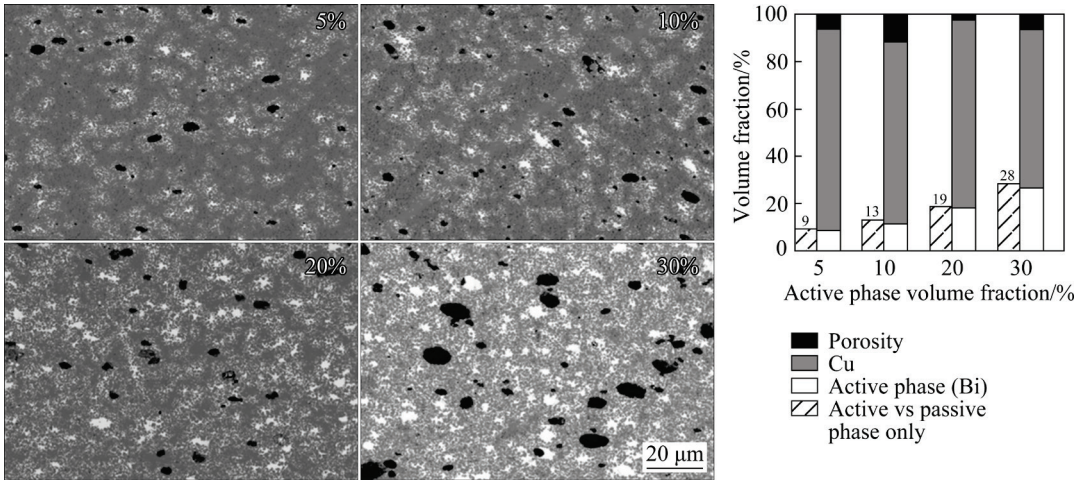

Fig. 7 SEM micrographs of Cu−Bi alloys with different nominal compositions (5%, 10%, 20% and 30% in volume fraction of Bi), and diagram showing volume factions of phases (Cu, Bi and porosity) measured from micrographs and percentage of active phase Bi with respect to Cu neglecting porosity indicated on plot

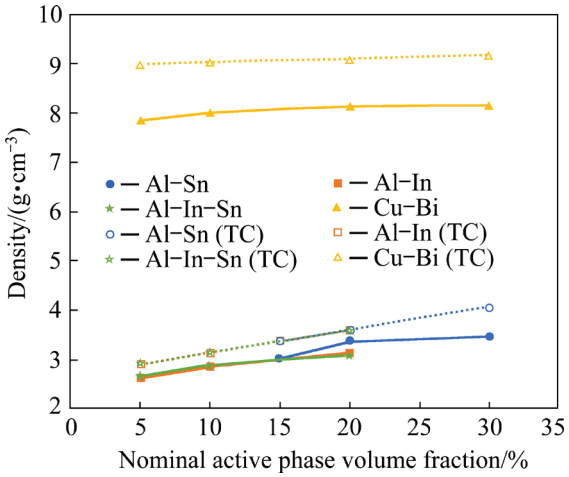

Fig. 8 Densities of different alloys as function of nominal active phase volume fraction (Solid lines indicate experimental results obtained with Archimedes' method and dashed lines represent theoretical values calculated with Thermo−Calc (TC))

the two elements are closer. Experimental values are 12%−14% lower than theoretical ones. For all the systems, Al-based as well as Cu−Bi alloys, the experimental density is always lower than theoretical density without a regular trend as function of active phase volume fraction.

3.2.3 Latent heat from DSC testing

Latent heat was evaluated with DSC tests in terms of onset temperature and energy. The curves of heat flow per unit mass as function of the temperature have V-shaped peaks in correspondence of melting during heating (upward) and solidification during cooling (downward) (Fig. 9).

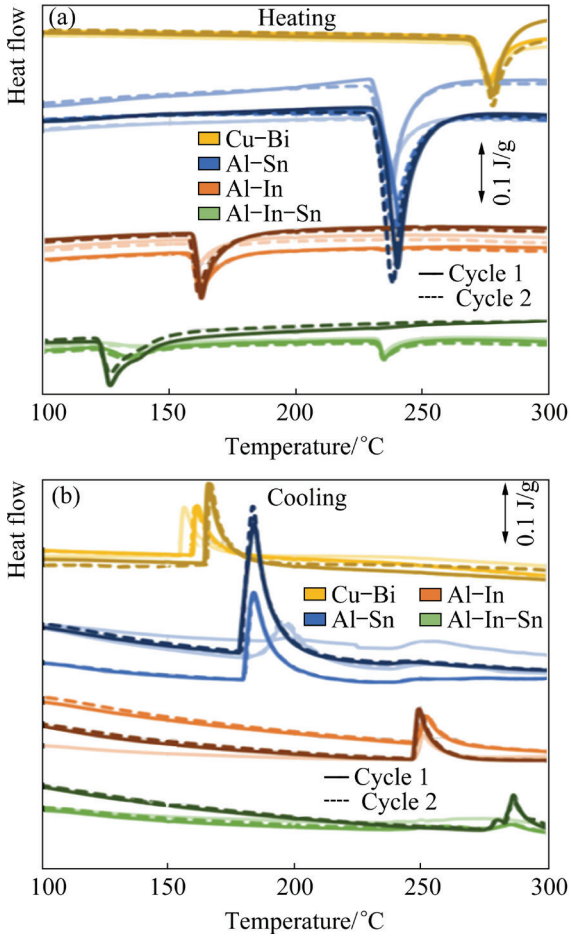

Fig. 9 Heat flow per unit mass as function of temperature for four produced systems (For each system, the quantity of active phase increases as the curve color becomes darker. For each alloy, curves corresponding to the two thermal cycles performed during the DSC test up to temperatures above melting are shown)

The onset of melting peaks corresponds to the expected temperatures for each system, while solidification peaks can show a certain degree on undercooling from a few degrees to 20−30 °C in the case of Cu−Bi. Curves of the first and second cycles performed during the test overlap quite well for all alloys. Focusing on Al−In−Sn curves corresponding to nominal 5% and 10% (volume fraction) of active phase (the ones in the lightest colors), they have a peak at about 120 °C, close to In−Sn eutectic temperature (117 °C) and a small second one at 229 °C, i.e., Sn melting temperature; on the other hand, the curve for 20% (volume fraction) nominal active phase has a single peak at about 120 °C. In cooling, all the Al−In−Sn alloys show peaks only close to 120 °C.

Comparing the measured latent heat with the calculated values obtained from Thermo−Calc (Fig. 10), experimental results are lower than those expected for their nominal composition.

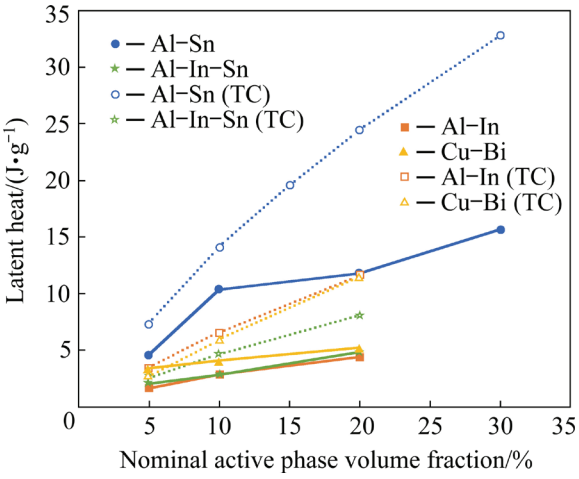

Fig. 10 Latent heat measured with DSC test (solid lines) and calculated with Thermo−Calc (TC, dashed lines) as function of nominal active phase volume fraction

3.2.4 Thermal expansion

The expansion per unit length measured with dilatometry tests is plotted as a function of temperature for some representative alloys in Fig. 11. The maximum expansion of Al-based alloys (Figs. 11(a, b)) was less than 1% (0.5%−0.6%) and, after the thermal cycle, the length of alloys returned to the initial length, or it was reduced by 0.1% or less; this reduction of specimen length was generally observed during the first thermal cycle, probably due to some adjustments of the phases and pores within the sample or of the sample itself within the machine, since a minimal compression load acted during the test. In the Al−Sn curves (Fig. 11(a)), it is also possible to see a little discontinuity in correspondence of the transition at 232 °C. Cu−Bi alloys (Fig. 11(c)) show a completely different behavior, with maximum expansion from 0.7% to 1.5%, and residual expansion from 0.3% to 1.1% after cycle.

The average values of the coefficient of thermal expansion (CTE) below and above transition temperature are compared in Fig. 12, as well as the CTE calculated by applying the mixture rule to the literature values available for the interval 0−100 °C (Table 1). For Al-based alloys, the experimental values below transition temperature are generally close to the expected values, i.e., 23−25 μm/(m·°C). Comparing the average CTE of Al-based alloys below and above transition temperature, they show negligible variations. Cu−Bi alloys have lower CTE with respect to Al-based ones, i.e., about 15 μm/(m·°C). The values below transition temperature match with calculated ones. On the other hand, above transition temperature, the CTE derived from experimental data increases significantly and has a much wider variation between

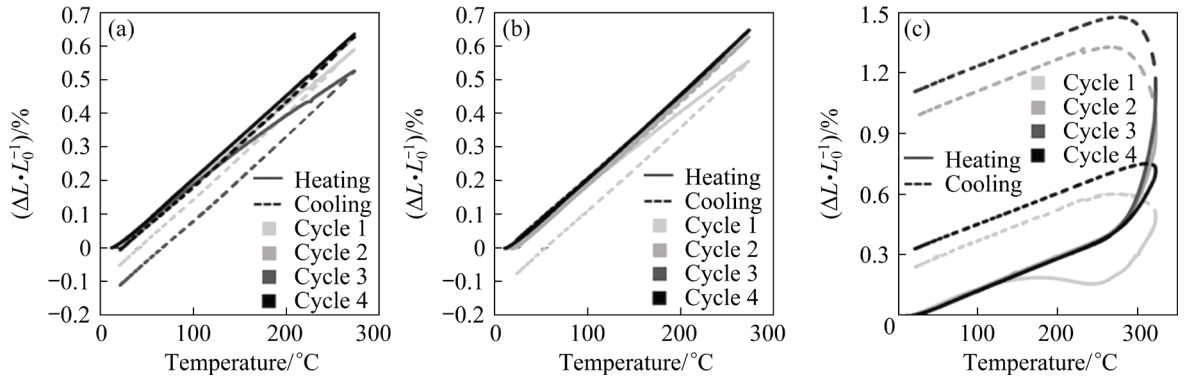

Fig. 11 Expansion per unit length as function of temperature for Al−10%Sn (a), Al−10%(In−Sn) (b) and Cu−10%Bi (c) measured with dilatometry test (Each specimen underwent four thermal cycles)

different thermal cycle repetitions.

3.2.5 Thermal diffusivity

The thermal diffusivity values measured with laser flash analysis (LFA) as a function of temperature for the four produced systems are shown in Fig. 13. Considering the overall trend, there is a good overlap of the curves in heating and cooling. In correspondence of or just before phase

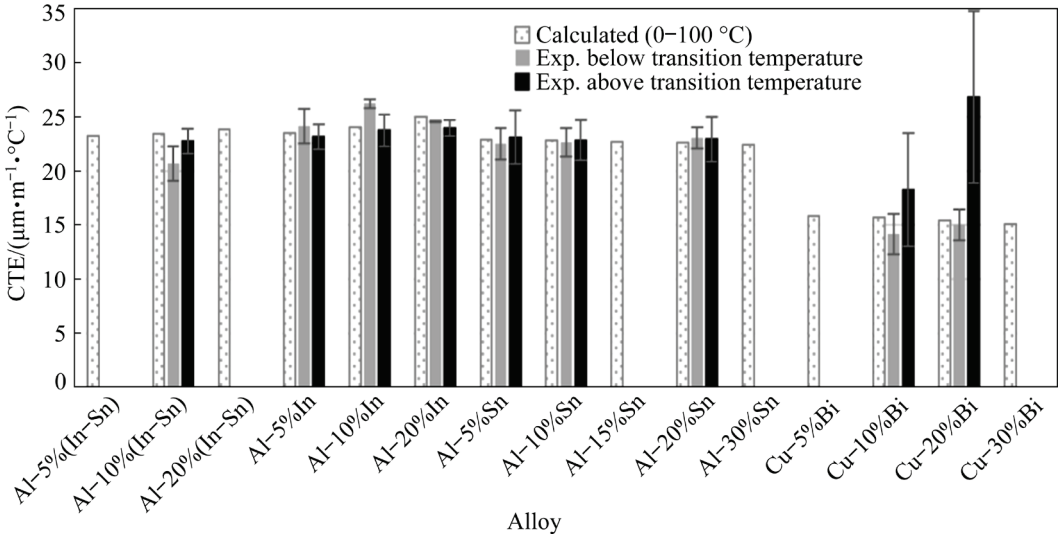

Fig. 12 CTE values of different alloys calculated from literature data and average CTE values measured below and above transition temperature

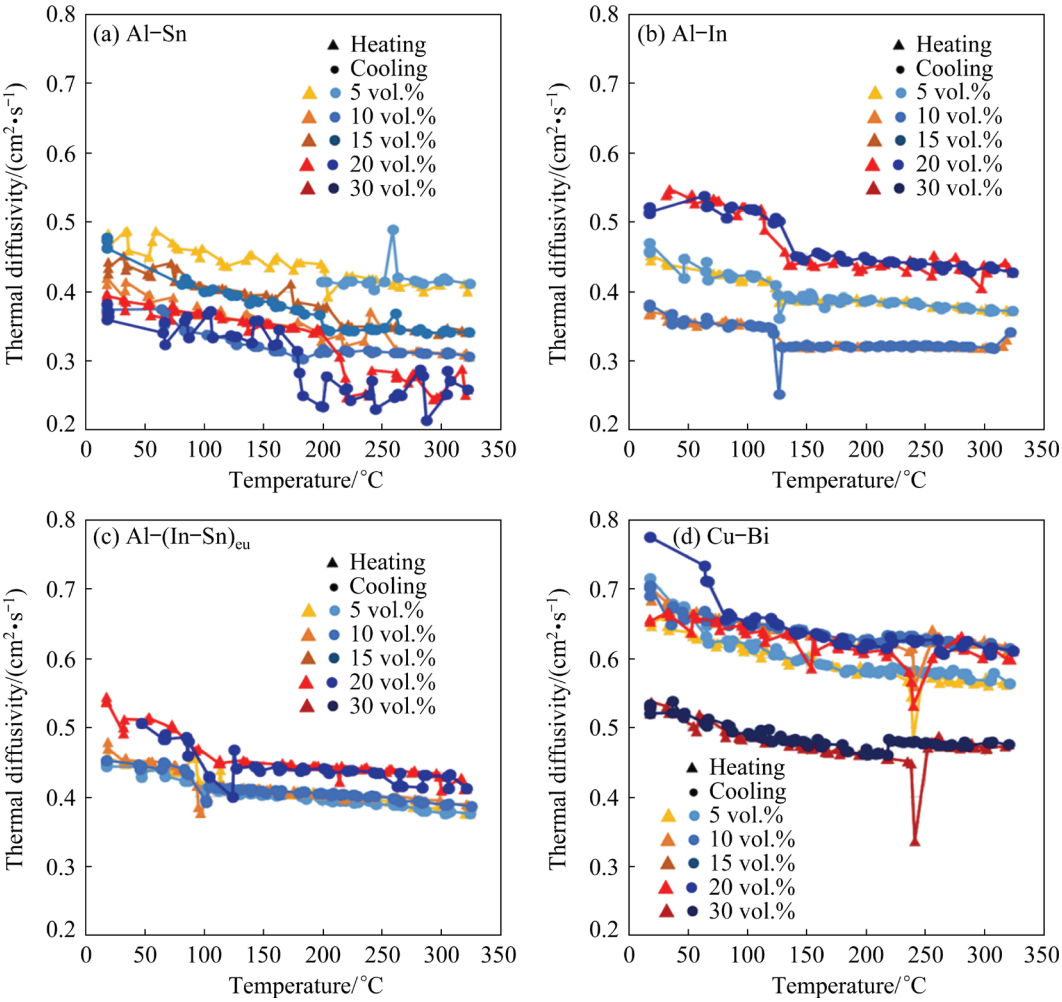

Fig. 13 Thermal diffusivity measured with LFA as function of temperature for four produced systems

transitions, there are step discontinuities in the curves. They are more evident for Al-based alloys, with a significant reduction of diffusivity after transition. Cu−Bi alloys, on the other hand, show a continuous and smooth decrease of diffusivity with increasing temperature, and a little upward step after transition. In addition, one or some points out of trend can be observed close to transition temperature. They can be correlated to the fact that, close to transition temperature the laser flash heat input on the sample causes its partial phase transition, so that the material is no longer homogeneous as initially assumed. The onset of phase transition changes heat transport conditions within the sample, resulting in a trend of the temperature increment on the opposite side of the sample not as expected (longer in heating conditions), thus reducing the indirectly measured thermal diffusivity according to LFA method. This phenomenon is related to the nature of PCM and will not be considered in further analysis.

Considering the diffusivity values as a function of nominal composition (volume fraction), a reduction of diffusivity with the active phase increase is expected for these systems, having the passive phase with higher diffusivity with respect to the active phase. While for Cu−Bi alloys, experimental thermal diffusivity is relatively close to expected values (Fig. 14), values for Al-based alloys are much lower and no trends are observed with the increase of the active phase nominal quantity.

3.2.6 Hardness

Vickers hardness values for all the tested alloys are shown in Fig. 15 as a function of nominal active phase volume fraction. Hardness of Cu−Bi alloys has a decreasing trend, from HV 70 to HV 43, as active phase volume fraction increases from 5% to 30%. Al-based alloys have lower hardness values with respect to Cu−Bi, which are between HV 20 and HV 30 with little variations for different contents of active phase. Contrary to Cu−Bi alloys, hardness values for Al-based alloys do not follow a clear trend and, considering also the standard variation indicated by the error bars, the measured hardness can be deemed as almost constant.

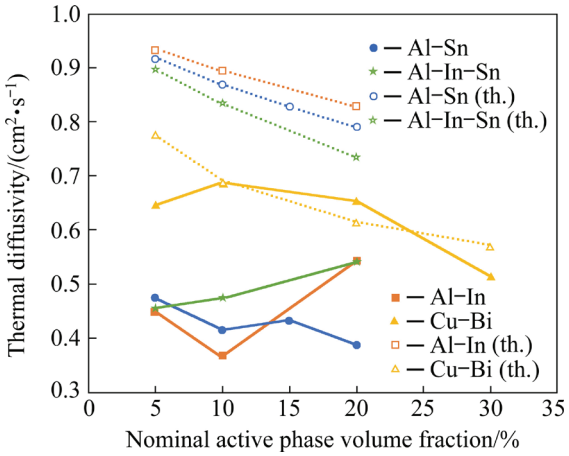

Fig. 14 Experimental (solid lines) and theoretical (th., dashed lines) thermal diffusivity at room temperature as function of nominal active phase volume fraction

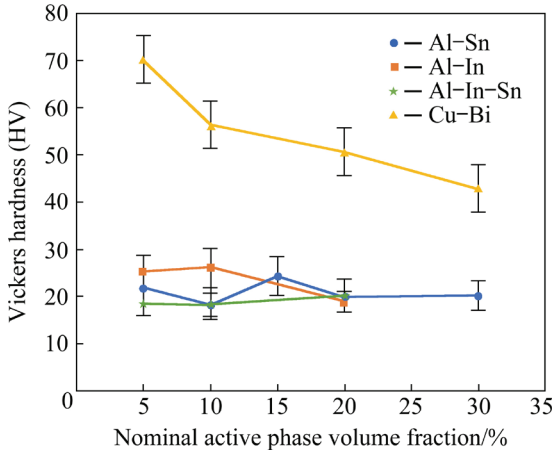

Fig. 15 Vickers hardness as function of nominal active phase volume fraction

4 Discussion

4.1 Calculated properties

Based on thermodynamic calculations, the proposed method for composite PCM design allows to compute several properties of interest in the full temperature range expected for service. The result is a detailed map of properties for many systems (Al−Bi, Al−In, Al−Sn, Cu−Bi, Al−In−Sn and Al−Bi−Sn) and compositions. Enthalpy-based calculations directly consider both contributions of latent heat and sensible heat to temperature-dependent storable energy. Storable energy in the full range of application temperature is closer to the behavior of a real component. Further, it allows comparisons among alloys with different transition temperatures working in the same temperature range. Applying this observation to the alloys studied in the present work, Al-based systems with different active phases show a quite similar heat storage per unit mass in temperature range of 100−300 °C (100−190 J/g, depending on the active

phase volume fraction) thanks to the high specific heat storable in Al. Thus, according to this analysis, it is possible to store the same overall amount of heat with the freedom to choose the active phase according to other specific application requirements, i.e., the transition temperature and the associated latent heat, but also, for example, thermal diffusivity or density.

Calculations with different active/passive phase ratios show that properties can vary with composition more or less significantly depending on the elements involved and their individual properties. For example, diffusivity at room temperature of Al−Bi and Al−Sn based alloys reduces more greatly than that of Al−In based alloys as active phase volume fraction decreases, thanks to the higher thermal diffusivity value for In with respect to the other two elements. The analysis of these trends can be important also in the definition of the production process, since it allows to evaluate how much local compositional variations are critical for the final material performance.

Calculations are particularly important when ternary alloys are considered; while properties of binary immiscible systems can be inferred quite precisely from pure element features, and the availability of suitable literature data for ternary immiscible alloys with specific composition is far more limited. Storable energy during transition is minimum for eutectic composition of active phase since it occurs at a constant temperature. Phase transitions at ipoeutectic and ipereutectic compositions also involve a specific heat contribution due to temperature change, so in these conditions the energy storage upon transition is more gradual as temperature increases and the storable heat is higher. This feature is less significant with compositions close to eutectic one (as shown for Al−Bi−Sn alloys) and if solidus and liquidus curves are close, as for Al−In−Sn system; this implies that small local variations of composition in the material can have only slight effects on the overall properties. Nevertheless, the overall storable energy in the temperature range of interest (100−300 °C) is the same for ternary alloys with the same passive/active phase volume fraction ratio, so the change in active phase composition only affects the heat storage mode.

4.2 Experimental results

The material characterization carried out in the present research displayed no interactions between active and passive phases for each selected system, as shown directly by EDS analyses and indirectly by DSC analysis, where peaks associated to active phase transitions occurred at expected temperatures. In the present study, chemical stability after few thermal cycles can be inferred from the overlapping of DSC curves in multiple cycle tests, since this confirms the absence of interactions that can change the curve shape in terms of shape, number and position of peaks. The overlapping of thermal diffusivity curves in heating and cooling in a temperature range assuring complete active phase melting is another point in favor of the compositional stability and the repeatability of material behavior over thermal cycles, which is the thermal stability of PCMs.

The unpredicted reaction observed between Al−Bi based alloys and water is attributed to the thermite reaction between Al, Bi_2O_3 and water, which uses hydrogen as intermediate product (causing the bubbles in water) [49]. In the preliminary literature analysis of the investigated systems, reactions of each single element oxides were not considered. Further, the papers specifically considered for Al−Bi based systems [4,50,51] did not report this problem, probably because they used casting processes and the bulk materials for casting were less affected by oxidation than powders. In the production method used in the present study, powder oxidation could occur and also, if powders are not completely compacted, they are more prone to react. This event will be considered as a lesson learnt about the preliminary analysis of possible chemical reactions, which will take into account more carefully the starting material and the environment of production process and service of C-PCMs. Nevertheless, Al−Bi based alloys will be still considered as promising C-PCMs, provided this potential issue is prevented in production process and application.

Comparing results of different tests, like density, phase quantities in micrographs, transition energy in DSC tests and thermal diffusivity, variations with respect to nominal compositions were directly or indirectly measured. These variations could be at least partially attributed to the presence of porosity. In addition, powder

metallurgy processes applied to a composite material could cause some inhomogeneity in sample composition affecting properties measured on small sample volumes, while the overall performance of the material follows the behaviour expected from nominal composition. In the present study, density measured on relatively big material volumes has values closer to the expected trends for each composition with respect to other properties measured on smaller volumes. Although production process will be carefully optimized to improve material homogeneity, the microstructure of metallic C-PCMs produced by powder metallurgy is anyway fine enough to be tested with the proposed methods and the obtained results can be analyzed to understand better material behavior despite the mismatches with nominal compositions.

Considering the active phase composition in the Al−In−Sn ternary alloy, micrographs and EDS analysis show a structure consisting of Sn primary grains with a eutectic or quasi-eutectic structure at grain boundaries. DSC curves show that the main transition peak is the one occurring at eutectic temperature, proving the capability of applied ball milling process to produce mechanical alloying of In and Sn. As an alternative, also atomization of powders directly from a master alloy of In−Sn eutectic composition could lead to homogeneous powder composition and microstructure. In addition, a peak at Sn melting temperature is observed as well in some curves. These results suggest the possibility of designing of a material with more than one active phase melting at different temperatures, which could be obtained by mixing powders with different compositions.

Focusing on microstructure, the presence of porosity was observed in all the alloys. According to micrographic analysis and density measurements, porosity variation with active phase quantity does not follow a regular trend. A regular trend could be expected considering that, reducing active phase volume fraction, the powder blend has higher quantities of hard particles (Al and Cu), which are less prone to plastically deform, thus leading to a less compact material. Also, the ambient conditions during compression, like temperature and especially humidity, can play a role in particle flow [52,53]. Finally, porosity can be related to molten phase motion due to capillary forces, as discussed for Cu−Bi. The root cause for porosity in the studied materials is probably a combination of all these phenomena. Porosity affects properties that depends on material volume, like density, thermal diffusivity and mechanical properties, generally reducing their values. Further, it can be useful to reduce tensions upon active phase expansion during melting, providing empty volume to be filled.

Microstructural analysis showed differences in phase arrangement among the alloys. This can be attributed to the different wettability features of the molten active phase on solid passive phase during sintering. When wettability is low, as in the case of the Al-based alloys, the powder metallurgy process results in the active phase embedded in the passive phase, without interconnections between active phase particles. On the other hand, the high wettability of Bi on Cu leads to continuous active phase network, where Bi-rich areas (reasonably former Bi powder particles) are surrounded by a network of Bi at Cu particles boundaries. Focusing on material properties, the most significant impact of molten phase wettability and phase arrangement was observed on thermal expansion evaluated in the dilatometric tests. Al-based alloys (about 0.6%) expand less than Cu−Bi alloys (1.5%) during a thermal cycle overcoming their melting range and their length is almost unchanged even after a few cycles, while Cu−Bi alloys keep a residual expansion (0.3%−1.1%). SINGH et al [54] attributed the expansion of Cu−Bi alloys before regular compressive creep behaviour to the penetration of liquid Bi in crevices of Cu particles, even breaking agglomerates, due to the capillary force enhanced by high wettability. These liquid motions also cause the formation of voids at the original location of Bi, thus explaining the porosity observed in as-sintered materials as well. These results suggest that continuous matrix of Al-based alloys and the low wettability of molten active phase on Al can keep the overall shape of the material even in the presence of loads without motion of liquid active phase in the solid structure. On the contrary, Cu−Bi alloys undergo more significant deformation even with a small load as in dilatometry tests (i.e., about 12 kPa); this behavior does not prevent the use of Cu−Bi system, but it should be taken into account in design step.

The presented analysis focused on heat storage and form-stability, but there is an additional function related to the phase transition, i.e., the

steep change of thermal diffusivity. Al-based alloys have a clear reduction after phase transition, while Cu−Bi alloys show a little increase. The difference between the two groups of alloys depends on the variation of thermal diffusivity of active phase with transition: In and Sn have a significant reduction of thermal conductivity upon solid−liquid transition, but Bi has a little increase [55,56]. In practical applications, this is an additional function of the material, since the change of thermal diffusivity affects the heat transfer rate in the material. Therefore, it is possible to use a metallic C-PCM to reduce or enhance heat transfer when the temperature of transition is reached.

5 Conclusions

(1) The calculations allowed to compare several systems with the freedom of choosing the desired composition, which includes not only the PCM, but the passive phase as well. Especially for ternary systems, this approach was useful to understand how different compositions affect the thermal behavior of a metallic C-PCM.

(2) The experimental testing of selected alloys showed that not all the features of interest can be simulated with these calculations, in particular the effect of microstructure and stability over thermal cycles. These two aspects are related to the phase distribution and the presence of porosity, which depend on production process, i.e., powder metallurgy for the investigated materials. The wettability of the molten active phase on the passive one plays a fundamental role in defining phase arrangement during production and properties in service conditions. Especially, both mechanical behavior and thermal conductivity are severely affected by the distribution of the low melting and low diffusivity active phase.

(3) The coupling of the theoretical and experimental approaches can ease and accelerate the development of metallic C-PCM, testing only the alloys with potentially suitable properties to evaluate experimentally the material features which cannot be simulated.

(4) This combination of approaches allows to analyze properties of C-PCMs from different perspectives, thus suggesting more ways to use these materials and how to control their performance in view of a tailored application to real components.

CRediT authorship contribution statement

Chiara CONFALONIERI: Conceptualization, Methodology, Investigation, Formal analysis, Data curation, Resources, Visualization, Writing – Original draft, Writing – Review & editing; **Alessandra CAMNAGHI:** Investigation, Formal analysis, Data curation; **Elisabetta GARIBOLDI:** Conceptualization, Methodology, Resources, Supervision, Writing – Review & editing.

Declaration of competing interest

The authors declare that they have no known competing financial interests or personal relationships that could have appeared to influence the work reported in this paper.

Data availability

The raw data and processed data required to reproduce these findings cannot be shared at this time as the data also forms part of an ongoing study.

Acknowledgments

The Italian Ministry of Education, University and Research is acknowledged for the support through the Project “Department of Excellence LIS4.0−Lightweight and Smart Structures for Industry 4.0”.

References

[1] RAGONE D V. Thermodynamics of materials (Volume I) [M]. New York: John Wiley & Sons Inc, 1995.

[2] LUCCHETTA M C, SAPORITI F, AUDEBERT F. Improvement of surface properties of an Al−Sn−Cu plain bearing alloy produced by rapid solidification [J]. Journal of Alloys and Compounds, 2019, 805: 709−717. doi: 10.1016/j.jallcom.2019.07.082.

[3] LU Z C, ZENG M Q, GAO Y, ZHU M. Significant improvement of wear properties by creating micro/nano dual-scale structure in Al−Sn alloys [J]. Wear, 2012, 296: 469−478. doi: 10.1016/j.wear.2012.08.002.

[4] SILVA A P, SPINELLI J E, MANGELINCK-NOËL N, GARCIA A. Microstructural development during transient directional solidification of hypermonotectic Al−Bi alloys [J]. Materials & Design, 2010, 31: 4584−4591. doi: 10.1016/j.matdes.2010.05.046.

[5] COSTA T A, FREITAS E S, DIAS M, BRITO C, CHEUNG N, GARCIA A. Monotectic Al−Bi−Sn alloys directionally solidified: Effects of Bi content, growth rate and cooling rate on the microstructural evolution and hardness [J]. Journal of Alloys and Compounds, 2015, 653: 243−254. doi: 10.1016/j.jallcom.2015.09.009.

[6] LIU X, ZENG M Q, MA Y, ZHU M. Promoting the high load-carrying capability of Al−20wt.%Sn bearing alloys

through creating nanocomposite structure by mechanical alloying [J]. Wear, 2012, 294/295: 387−394. doi: 10.1016/j.wear.2012.07.021.

[7] MAKHATHA M E, FATOBA O S, AKINLABI E T. Effects of rapid solidification on the microstructure and surface analyses of laser-deposited Al−Sn coatings on AISI 1015 steel [J]. The International Journal of Advanced Manufacturing Technology, 2018, 94: 773−787. doi: 10.1007/s00170-017-0876-y.

[8] STUCZYÑSKI T. Metallurgical problems associated with the production of aluminium-tin alloys [J]. Materials & Design, 1997, 18: 369−372. doi: 10.1016/S0261-3069(97)00078-2.

[9] NING X J, KIM J H, KIM H J, LEE C. Characteristics and heat treatment of cold-sprayed Al−Sn binary alloy coatings [J]. Applied Surface Science, 2009, 255: 3933−3939. doi: 10.1016/j.apsusc.2008.10.074.

[10] RAN G, ZHOU J E, XI S, LI P. Microstructure and morphology of Al−Pb bearing alloy synthesized by mechanical alloying and hot extrusion [J]. Journal of Alloys and Compounds, 2006, 419: 66−70. doi: 10.1016/j.jallcom.2005.09.057.

[11] CAO C, LIU W, LIU Z, XU J, HWANG I, de ROSA I, LI X. Scalable manufacturing of immiscible AlBi alloy by self-assembled nanoparticles [J]. Materials & Design, 2018, 146: 163−171. doi: 10.1016/j.matdes.2018.03.008.

[12] YUAN G, LI Z, LOU Y, ZHANG X. Study on crystallization and microstructure for new series of Al−Sn−Si alloys [J]. Materials Science and Engineering: A, 2000, 280: 108−115. doi: 10.1016/S0921-5093(99)00675-9.

[13] ZHAI W, HU L, GENG D L, WEI B. Thermodynamic properties and microstructure evolution of ternary Al−10%Cu−*x*%Sn immiscible alloys [J]. Journal of Alloys and Compounds, 2015, 627: 402−409. doi: 10.1016/j.jallcom.2014.11.191.

[14] BHAT J, PINTO R, SATYANARAYAN S. A review on effect of alloying elements and heat treatment on properties of Al−Sn alloy [J]. Materials Today: Proceedings, 2021, 35: 340−343. doi: 10.1016/j.matpr.2020.01.617.

[15] YUAN K, SHI J, AFTAB W, QIN M, USMAN A, ZHOU F, LV Y, GAO S, ZOU R. Engineering the thermal conductivity of functional phase−change materials for heat energy conversion, storage, and utilization [J]. Advanced Functional Materials, 2020, 30: 1904228. doi: 10.1002/adfm.201904228.

[16] SINGH S P, DEB BARMAN B K, KUMAR P. Cu−Bi alloys with high volume fraction of Bi: A material potentially suitable for thermal surge protection and energy storage [J]. Materials Science and Engineering: A, 2016, 677: 140−152. doi: 10.1016/J.MSEA.2016.09.041.

[17] CONFALONIERI C, LI Z, GARIBOLDI E. Metallic form-stable phase change materials for thermal energy storage and management: General features and effect of manufacturing process on thermal response and stability [J]. International Journal of the Italian Association for Metallurgy, 2019, 111: 12−20. http://www.aimnet.it/la_metallurgia_ italiana/2019/luglioagosto/Gariboldi.pdf.

[18] SUGO H, KISI E, CUSKELLY D. Miscibility gap alloys with inverse microstructures and high thermal conductivity for high energy density thermal storage applications [J]. Applied Thermal Engineering, 2013, 51: 1345−1350. doi: 10.1016/J.APPLTHERMALENG.2012.11.029.

[19] ZHOU C, WU S K. Medium- and high-temperature latent heat thermal energy storage: Material database, system review, and corrosivity assessment [J]. International Journal of Energy Research, 2019, 43: 621−661. doi: 10.1002/er.4216.

[20] WEI G, WANG G, XU C, JU X, XING L, DU X, YANG Y. Selection principles and thermophysical properties of high temperature phase change materials for thermal energy storage: A review [J]. Renewable and Sustainable Energy Reviews, 2018, 81: 1771−1786. doi: 10.1016/J.RSER.2017.05.271.

[21] COSTA S C, KENISARIN M. A review of metallic materials for latent heat thermal energy storage: Thermophysical properties, applications, and challenges [J]. Renewable and Sustainable Energy Reviews, 2022, 154: 111812. doi: 10.1016/j.rser.2021.111812.

[22] WANG S, LEI K, WANG Z, WANG H, ZOU D. Metal-based phase change material (PCM) microcapsules/nanocapsules: Fabrication, thermophysical characterization and application [J]. Chemical Engineering Journal, 2022, 438: 135559. doi: 10.1016/j.cej.2022.135559.

[23] RAWSON A J, KRAFT W, GLÄSEL T, KARGL F. Selection of compatible metallic phase change materials and containers for thermal storage applications [J]. Journal of Energy Storage, 2020, 32: 101927. doi: 10.1016/j.est.2020.101927.

[24] GHERIBI A E, PELTON A D, HARVEY J P. Determination of optimal compositions and properties for phase change materials in a solar electric generating station [J]. Solar Energy Materials and Solar Cells, 2020, 210: 110506. doi: 10.1016/j.solmat.2020.110506.

[25] REED R C, ZHU Z, SATO A, CRUDDEN D J. Isolation and testing of new single crystal superalloys using alloys-by-design method [J]. Materials Science and Engineering: A, 2016, 667: 261−278. doi: 10.1016/j.msea.2016.04.089.

[26] GARIBOLDI E, PERRIN M. Metallic composites as form-stable phase change alloys [J]. Materials Science Forum, 2018, 941: 1966−1971. doi: 10.4028/www.scientific.net/MSF.941.1966.

[27] CONFALONIERI C, BASSANI P, GARIBOLDI E. Microstructural and thermal response evolution of metallic form-stable phase change materials produced from ball-milled powders [J]. Journal of Thermal Analysis and Calorimetry, 2020, 142: 85−96. doi: 10.1007/s10973-020-09785-7.

[28] CONFALONIERI C, GARIBOLDI E. Al−Sn miscibility gap alloy produced by power bed laser melting for application as phase change material [J]. Journal of Alloys and Compounds, 2021, 881: 160596. doi: 10.1016/j.jallcom.2021.160596.

[29] MARROCCO T, DRIVER L C, HARRIS S J,

MCCARTNEY D G. Microstructure and properties of thermally sprayed Al−Sn-based alloys for plain bearing applications [J]. Journal of Thermal Spray Technology, 2006, 15: 634−639. doi: 10.1361/105996306X147009.

[30] CHIKOVA O A, KONSTANTINOV A N, SHISHKINA E V, CHEZGANOV D S. Nanoindentation study of the effect of the structural state of the melt on the crystal structure and mechanical properties of the phases in an Al−50wt.%Sn alloy [J]. Russian Metallurgy (Metally), 2013, 2013: 535−544. doi: 10.1134/S0036029513070045.

[31] ANDERSSON J O, HELANDER T, HÖGLUND L, SHI P, SUNDMAN B. Thermo-Calc & DICTRA, computational tools for materials science [J]. Calphad, 2002, 26: 273−312. doi: 10.1016/S0364-5916(02)00037-8.

[32] Thermo-Calc Software TCAL5.1. Al-alloys database [EB/OL]. 2020−06−15. https://thermocalc.com.2020.

[33] FIEDLER T, BELOVA I V, MURCH G E. Theoretical and lattice monte carlo analyses on thermal conduction in cellular metals [J]. Computational Materials Science, 2010, 50: 503−509. doi: 10.1016/j.commatsci.2010.09.011.

[34] KIRADJIEV K B, HALVORSEN S A, van GORDER R A, HOWISON S D. Maxwell-type models for the effective thermal conductivity of a porous material with radiative transfer in the voids [J]. International Journal of Thermal Sciences, 2019, 145: 106009. doi: 10.1016/j.ijthermalsci. 2019.106009.

[35] ORDÓÑEZ-MIRANDA J, ALVARADO-GIL J J, MEDINA-EZQUIVEL R. Generalized Bruggeman formula for the effective thermal conductivity of particulate composites with an interface layer [J]. International Journal of Thermophysics, 2010, 31: 975−986. doi: 10.1007/ s10765-010-0756-2.

[36] PROGELHOF R C, THRONE J L, RUETSCH R R. Methods for predicting the thermal conductivity of composite systems: A review [J]. Polymer Engineering and Science, 1976, 16: 615−625. doi: 10.1002/pen.760160905.

[37] RAWSON A J, KISI E, WENSRICH C. Microstructural efficiency: Structured morphologies [J]. International Journal of Heat and Mass Transfer, 2015, 81: 820−828. doi: 10.1016/j.ijheatmasstransfer.2014.11.012.

[38] CARDARELLI F, CARDARELLI F. Materials handbook [M]. 2nd ed. London: Springer, 2008: 159−212.

[39] SHACKELFORD W, ALEXANDER W. CRC materials science and engineering handbook [M]. 3rd ed. Boca Raton: CRC Press, 2001. doi: 10.1201/9781420038408

[40] GUNN G. Critical metals handbook [M]. Chickester, UK: John Wiley & Sons, Ltd, 2014.

[41] MatWeb. Bismuth [EB/OL]. 2020−07−16. http://www. matweb.com/search/DataSheet.aspx?MatGUID=09436237bf 3c4067a2bb210cb02c31b5&ckck=1.

[42] MatWeb. Indium [EB/OL]. 2020−07−16. https://www. matweb.com/search/DataSheet.aspx?MatGU.

[43] GARIBOLDI E, LI Z, RAWSON A J. Effective thermal conductivity in BCC and FCC lattices for all volume fractions and conductivity ratios: Analyses by microstructural efficiency and morphology factor and analytic models [J]. Materials Today Communications, 2022, 33: 104253. doi: 10.1016/j.mtcomm.2022.104253.

[44] ASTM E228, Standard test method for linear thermal expansion of solid materials with a push-rod dilatometer [S]. 2017.

[45] OKAMOTO H. Al−In (aluminum−indium) [J]. Journal of Phase Equilibria and Diffusion, 2012, 33: 413−413. doi: 10.1007/s11669-012-0074-4.

[46] PREDEL B. Al−Sn (aluminum−tin): Datasheet from Landolt−Börnstein−Group IV Physical Chemistry Volume 5A: "Ac−Au–Au−Zr" [C]//Heidelberg: Springer, 1991. doi: 10.1007/10000866_144.

[47] LIU Y, TU K N. Low melting point solders based on Sn, Bi, and In elements [J]. Materials Today Advances, 2020, 8: 100115. doi: 10.1016/j.mtadv.2020.100115.

[48] UNDERWOOD E E. The mathematical foundations of quantitative stereology [C]// Stereology and Quantitative Metallography. West Conshohocken, PA: ASTM International, 1972: 3–38. doi: 10.1520/STP36841S.

[49] PUSZYNSKI J A, BULIAN C J, SWIATKIEWICZ J J. Processing and ignition characteristics of aluminum−bismuth trioxide nanothermite system [J]. Journal of Propulsion and Power, 2007, 23: 698−706. doi: 10.2514/1.24915.

[50] BERTELLI F, CHEUNG N, FERREIRA I L, GARCIA A. Evaluation of thermophysical properties of Al–Sn–Si alloys based on computational thermodynamics and validation by numerical and experimental simulation of solidification [J]. The Journal of Chemical Thermodynamics, 2016, 98: 9–20. doi: 10.1016/j.jct.2016.02.018.

[51] KHAN A, MATLI P R, NAWAZ M, MATTLI M R, PARANDE G, MANAKARI V, SHAKOOR A, ALJABER A S, GUPTA M. Microstructure and mechanical behavior of hot extruded aluminum/tin−bismuth composites produced by powder metallurgy [J]. Applied Sciences, 2020, 10: 2812. doi: 10.3390/app10082812.

[52] GORDON D, WHITTAKER D. Introduction to powder metallurgy [C]//European Powder Metallurgy Association (EPMA). Shrewsbury, UK, 2008.

[53] MARCHETTI L, MELLIN P, HULME C N. Negative impact of humidity on the flowability of steel powders [J]. Particulate Science and Technology, 2022, 40: 722–736. doi: 10.1080/02726351.2021.1995091.

[54] SINGH S P, SONAWANE D, KUMAR P. Creep of Cu−Bi alloys with high Bi content near and above melting temperature of Bi [J]. Metallurgical and Materials Transactions A, 2019, 50: 2690−2701. doi: 10.1007/ s11661-019-05206-z.

[55] PERALTA-MARTINEZ M V, WAKEHAM W A. Thermal conductivity of liquid tin and indium [J]. International Journal of Thermophysics, 2001, 22: 395–403. doi: 10.1023/A:1010714612865.

[56] KRZHIZHANOVSKII R E, SIDOROVA N P, BOGDANOVA I A. Experimental investigation of the electrical resistivity of some molten bismuth−tin binary alloys and of the thermal conductivity of bismuth, tin, and a eutectic bismuth−tin alloy [J]. Journal of Engineering Physics, 1974, 26: 33−36. doi: 10.1007/BF00827284.

从热力学计算到定形体系的实验表征设计全金属复合相变材料

Chiara CONFALONIERI, Alessandra CAMNAGHI, Elisabetta GARIBOLDI

Politecnico di Milano, Department of Mechanical Engineering, Via La Masa 1, 20156 Milan, Italy

摘　要：用于热能管理的复合相变材料(C-PCMs)利用其一个或多个低熔点活性相的可逆相变（如熔化—凝固）存储和释放热能作为潜热。同时，高熔点的惰性相可以提供额外的性能，如定形性和改善的导热性。从难混溶合金中可获得具有这些特征的全金属复合材料体系。本文将热力学计算和实验测试相结合，探讨二元(Al−In, Al−Sn, Al−Bi 和 Cu−Bi)和三元(Al−In−Sn 和 Al−Bi−Sn) 难混溶合金在 100~300 ℃的温度范围内用作 C-PCMs 的潜力。结果表明，将这两种方法相结合对于全面理解复合体系和找到满足设计需求的最佳解决方案十分必要，它克服了“试错”法浪费时间的弊端，并为模拟提供了高质量的数据。

关键词：复合相变材料；合金设计；热力学性能；定形性；储热

(Edited by Wei-ping CHEN)